

Density Profiles of Liquid/Vapor Interfaces Away from Their Critical Points

Wei Bu¹, Doseok Kim² and David Vaknin^{1*}

¹*Ames Laboratory and Department of Physics and Astronomy, Iowa State University, Ames, Iowa 50011, USA*

²*Department of Physics, Sogang University, Seoul 121-742, Korea*

(Dated: April 30, 2014)

We examine the applicability of various model profiles for the liquid/vapor interface by X-ray reflectivities on water and ethanol and their mixtures at room temperature. Analysis of the X-ray reflectivities using various density profiles shows an error-function like profile is the most adequate within experimental error. Our finding, together with recent observations from simulation studies on liquid surfaces, strongly suggest that the capillary-wave dynamics shapes the interfacial density profile in terms of the error function.

PACS numbers:

I. INTRODUCTION

The density profiles of the liquid/vapor interfaces have been the subject of intense investigations theoretically [1–7] and experimentally [8–11] for over a century by now. Near the gas/vapor critical temperature, the thickness of the interface varies from hundreds to thousands of Angstroms (Å) [8–10], whereas, it is only a few Å thick away from the critical temperature [12, 13]. It is by now accepted that the effective thickness of the liquid/vapor profile is dominated by capillary waves [14–17] with a smaller contribution from intrinsic roughness. The intrinsic roughness arises from the discreteness of molecules forming the liquid [18]. However, the form of the functional density profile at the interface has not been systematically addressed.

Several possible density profiles, such as, the hyperbolic tangent function, based on mean-field theory [1, 2] and the error function, associated with capillary wave theory [4], have been proposed. Liquid/vapor interface undergoing fluctuation due to thermal capillary wave has been investigated quantitatively by molecular dynamics simulations [19, 20]. In these studies, two different functions (error- and hyperbolic-tangent-function) were used to fit the interfacial density profile obtained from the simulations. The surface tension could be calculated from the derivatives of the above functions, which then were compared with the surface tension deduced from the pressure difference at the interface. The above two surface tension values were shown to agree better when the density profile was modeled by the error function than the hyperbolic tangent function. However, a more recent molecular-dynamics (TIP4P-QDP-LJ model) simulations result demonstrates that both the error and hyperbolic tangent functions adequately fit the density profile [21].

Light scattering investigations of the profile close to the critical point have been thoroughly addressed by Huang, Wu, and Webb [9, 10] who had shown that the hyperbolic tangent profile can be excluded based on the analysis of critical exponent predictions that favored two closely related profiles (i.e. error function and the Fisk-Widom profile) [9, 10]. Although, away from the critical point,

the error function has always been assumed as the interfacial shape in many X-ray and neutron scattering experiments, there has not been a systematic examination to compare the applicability of other profiles.

Since the liquid/vapor interface of simple liquids is typically a few angstroms wide far from the critical point, X-ray reflectivity technique is most suitable to determine the interfacial profile at this length scale. In this manuscript, we report synchrotron X-ray reflectivities on various liquid/gas interfaces far below the critical point of two liquids and their mixtures, to examine the applicability of possible profiles that best fit the experimental data.

II. THEORETICAL BACKGROUND

A. Possible density profiles

X-ray reflectivity probes the electron density (ED) profile along the interfacial normal which, to a good approximation, can be related to the molecular density profile. We will therefore assume that the ED profile represents the density profile from this point on. We label the ED values ρ_1 and ρ_2 for the electron densities of the gas and the liquid away from the interface, respectively. The interfacial profile can then be written, in density language, as

$$\rho(z) = \frac{1}{2} [(\rho_1 + \rho_2) - (\rho_1 - \rho_2)f(z)], \quad (1)$$

where z is the direction normal to the interfacial plane, and f is a universal monotonic function such that $f(\pm\infty) = \pm 1$. In the present study, $\rho_1 \approx 0$ and by denoting $\rho_s = \rho_2$, Eq. (1) can be simplified as follows

$$\rho(z) = \frac{\rho_s}{2} (1 + f(z)). \quad (2)$$

For the ideally flat surface (i.e., zero interfacial thickness), with step-function-like profile (i.e., $f(z) = \text{sign}(z)$ with values 1 and -1 for $z > 0$ and $z < 0$, respectively, and $(1 + f(z))/2 \equiv \Theta(z)$), the corresponding X-ray reflectivity is the so-called Fresnel reflectivity (R_F). The

nonzero profile-width results in a departure of the reflectivity from the Fresnel reflectivity, as discussed below.

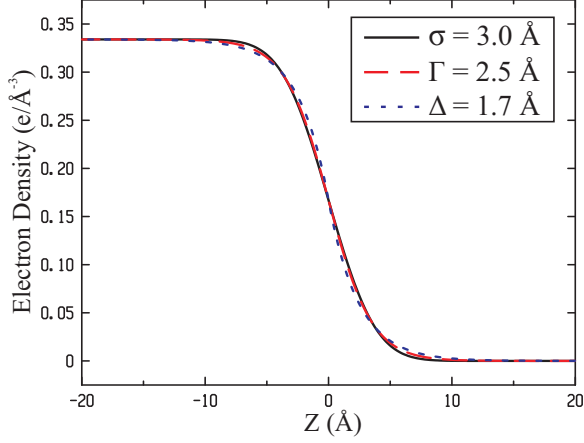


FIG. 1: (Color online) ED profiles constructed by the error-, hyperbolic-tangent-, and exponential-functions of widths σ , Γ , and Δ respectively, with the same exchange length $L = 3.0$ Å, as discussed in the text. Here, $\rho_s = 0.334$ e/Å³ represents the ED of pure water.

In the mean-field theory near the gas/liquid critical point the profile is $f(z) = \tanh(\frac{z}{\sqrt{2}\Gamma})$, (TANH), as first derived by van der Waals and Cahn-Hilliard theory [1, 2]. Employing capillary wave-theory, Buff, Lovett, and Stillinger [4] predicted the profile of the interface is an error-function $f(z) = \text{erf}(\frac{z}{\sqrt{2}\sigma})$ (ERF), where σ is the surface roughness. We compare experimental results to the two profiles, and for further comparison also examine the profile produced by the exponential function (EXP) as follows.

$$\begin{aligned} f(z) &= \exp(\frac{z}{\sqrt{2}\Delta})/2, \quad z < 0 \\ &= 1 - \exp(\frac{-z}{\sqrt{2}\Delta})/2, \quad z > 0 \end{aligned} \quad (3)$$

The roughness parameters σ , Γ , and Δ of the different profile functions, are all related through an average profile width by the exchange length [9], defined by

$$L = \sqrt{\frac{\pi}{2}} \int_0^\infty (1 - f(z)) dz, \quad (4)$$

which yields $L = \sigma = \ln 2 \sqrt{\pi} \Gamma = \sqrt{\pi} \Delta$, providing a basis for comparing different profile functions. Figure 1 shows ED profiles constructed by ERF (solid line), TANH (dashed line) and EXP (dotted line) with the same exchange length; ($L = \sigma = 3.0$ Å; typical value for the water/vapor interface at room temperature)[18], indicating the three line are almost indistinguishable.

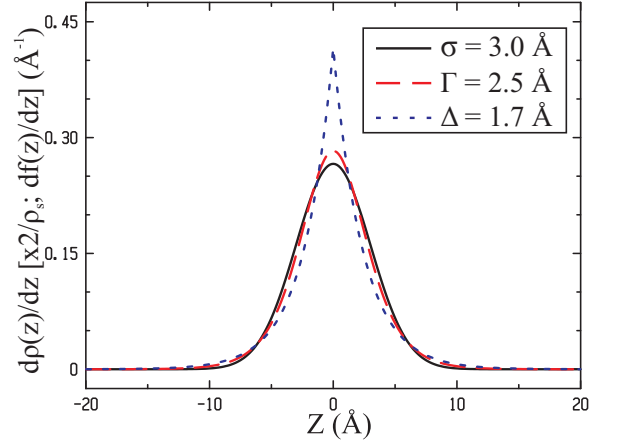


FIG. 2: (Color online) Derivatives of corresponding ED profiles shown in Fig. 1.

B. X-ray Reflectivity

X-ray reflectivity from an ideally flat surface (step-like function) can be analytically solved by using Helmholtz equation and the boundary conditions at the interface $z = 0$. This is usually referred to as the Fresnel reflectivity which is given by

$$R_F = \left| \frac{Q_z - Q_s}{Q_z + Q_s} \right|^2, \quad (5)$$

where Q_z is the momentum transfer along z , and $Q_s = \sqrt{Q^2 - 16\pi\rho_s r_0}$ (r_0 is radius of electron). For $Q_z \gg Q_c$ (above the critical angle for total reflection, $Q_c \equiv \sqrt{16\pi\rho_s r_0}$), the Fresnel reflectivity (Eq. (5)) can be simplified to $R_F \approx 16\pi^2 \rho_s^2 r_0^2 / Q_z^4$.

For a more structured profile (non-step-like profile), the X-ray reflectivity can be exactly calculated by applying the recursive dynamical method [22] by slicing the ED profile [23] (i.e. ERF, TANH, and EXP). Alternatively, the reflectivity can be calculated with high accuracy, especially for $Q_z \gg Q_c$, in the Distorted Wave Born approximation (DWBA), such that,

$$R = R_F \left| \int \frac{d\rho(z)}{dz} \exp(iQ_z z) dz \right|^2, \quad (6)$$

Thus, substituting the derivative of the step function, $d\rho(z)/dz = \rho_s \delta(z)$, into Eq. (6) simply yields the Fresnel Reflectivity R_F . Herein, we apply the exact and the DWBA methods.

As expressed in Eq. (6) the reflectivity depends on the derivative of the ED profile. Derivatives of the ED profiles constructed by ERF, TANH, and EXP, are listed

as below,

$$\frac{d\rho(z)}{dz} = \frac{\rho_s}{\sqrt{2\pi}\sigma} \exp\left(-\frac{z^2}{2\sigma^2}\right), \quad (7a)$$

$$\frac{d\rho(z)}{dz} = \frac{\rho_s}{2\sqrt{2}\Gamma} \frac{1}{\cosh^2\left(\frac{z}{\sqrt{2}\Gamma}\right)}, \quad (7b)$$

$$\frac{d\rho(z)}{dz} = \frac{\rho_s}{2\sqrt{2}\Delta} \exp\left(\frac{-|z|}{\sqrt{2}\Delta}\right), \quad (7c)$$

and example calculations are shown in Fig. 2. Although the corresponding ED profiles shown in Fig. 1 are hard to distinguish, their derivatives are quite different, especially for the EXP function.

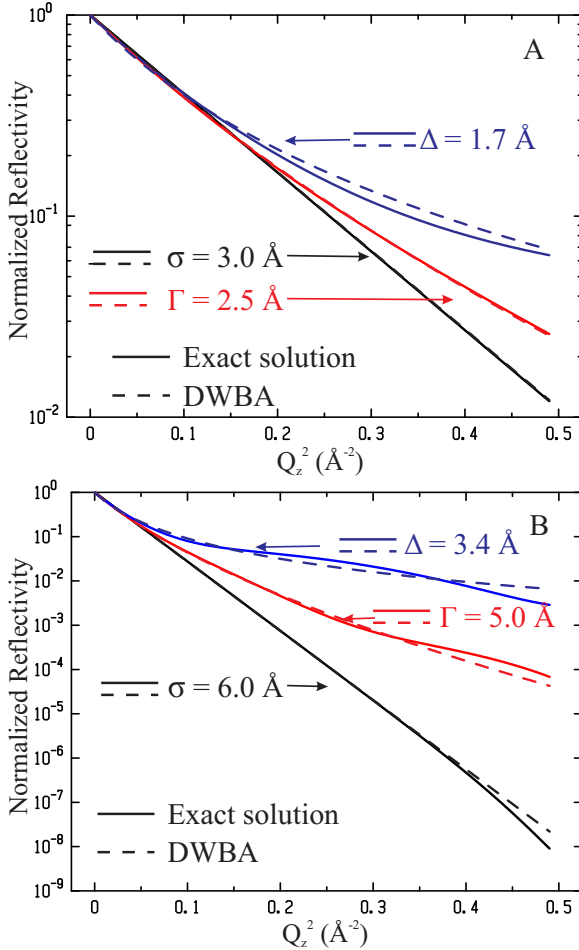


FIG. 3: (Color online) Calculated normalized reflectivities of corresponding ED profiles shown in Fig. 1 are plotted *versus* Q_z^2 . Solid lines and dashed lines represent the exact solution obtained using recursive dynamics method and DWBA, respectively.

Substitution of Eq. (7) into Eq. (6) and using the definition of R_F in Eq. (6) gives the normalized reflectivities

$$\frac{R}{R_F} = \exp(-Q_z^2 \sigma^2), \quad (8a)$$

$$\frac{R}{R_F} = \left[\frac{\Gamma Q_z \pi}{\sqrt{2} \sinh\left(\frac{\Gamma Q_z \pi}{\sqrt{2}}\right)} \right]^2, \quad (8b)$$

$$\frac{R}{R_F} = \left[\frac{1}{1 + 2Q_z^2 \Delta^2} \right]^2. \quad (8c)$$

One should notice that the normalized reflectivities, R/R_F , are independent of subphase ED (ρ_s). Figure 3 shows normalized reflectivities calculated by recursive dynamical method (solid lines) and Born approximation (dashed lines) for the corresponding ED profiles shown in Fig. 1. The calculated reflectivities using the two different methods are practically indistinguishable for ERF and TANH ED profiles when $L = 3.0$ Å, whereas the EXP profile differs slightly between the two methods. As for the density profile, deviation of the EXP profile from the other two is appreciable for large Q_z values. By contrast, at larger L (Fig. 3 for $L = 6.0$ Å), the three profiles give very different reflectivities even at small Q_z values. Note, that calculated reflectivities for TANH and EXP ED profiles are about four to six orders of magnitude larger than the one with ERF ED profile at large Q_z , respectively.

III. EXPERIMENTAL DETAILS

The X-ray reflectivity experiments were conducted on the Ames Laboratory Liquid Surface Diffractometer at the 6ID-B beamline at the Advanced Photon Source (APS) at Argonne National Laboratory [24]. The highly monochromatic beam (16.2 keV; $\lambda = 0.765335$ Å), selected by an initial Si double crystal monochromator, is deflected onto the liquid surface at a desired angle of incidence with respect to the liquid surface by a second monochromator (Ge(220) single crystal), which is placed on the diffractometer [24]. High beam flux can provide reflectivity data with good statistics up to $Q_z \sim 0.8$ Å⁻¹.

Ultrapure water (Millipore, Milli-Q, and NANOpure, Barnstead; resistivity, 18.1 MΩcm) and ethanol (99.5 %, Fisher) were used for all subphase preparations. Solutions were contained in a stainless steel trough with the depth of 0.3 mm to reduce the effect of mechanical agitations on the surface smoothness. To test the quality of the surface we routinely checked that the reflection from the surface below the critical angle is nearly 100% (i.e., total reflection). The trough was encapsulated in an air-tight thermostatic aluminum enclosure ($T = 293$ K), which was continuously purged with a helium gas flow (bubbled through the same mixture as the sample) during the course of the experiment to lower background scattering from the air.

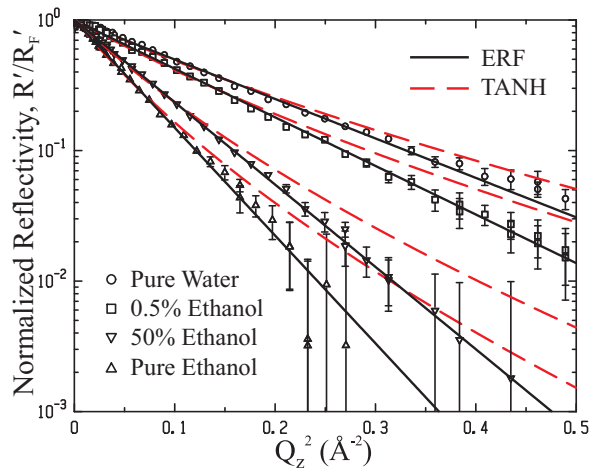


FIG. 4: (Color online) Normalized reflectivities (R/R_F) of pure water (circles), 0.5% ethanol (squares), 50% ethanol (inverted triangles), and pure ethanol (triangles). Solid and dashed lines are the best fits by considering ERF or TANH as ED profiles, respectively.

IV. RESULTS AND DISCUSSIONS

TABLE I: Parameters that generate the best-fit calculated reflectivities to the experimental data in Fig. 4.

subphase	σ (Å)	Γ (Å)	σ/Γ
pure water	2.64	2.18	1.21
0.5% ethanol	2.93	2.43	1.20
50% ethanol	3.81	3.20	1.19
pure ethanol	4.36	3.62	1.21

As discussed above and shown in Fig. 3, large roughness ($L > 3.0$ Å) is necessary to test the adequacy of the ERF and TANH ED profiles in modeling the measured reflectivities. Pure ethanol at room temperature has much lower surface tension (ST; ~ 23 mN/m) than that of pure water (≈ 73 mN/m), inducing thermally excited capillary waves with adequate roughness to test the various ED profiles. Thus, water and ethanol mixtures have been used here for increasing the roughness gradually by increasing the ethanol portion in the mixture. The other apparent way to gradually change interfacial tension is to form and compress a Langmuir monolayer, however such a system is more complicated as it introduces distinct layering at the interface and requires extra fitting parameters[23], while the mixture-bare-interface is a simpler surface that can be adequately modeled by Eq. (8). Figure 4 shows normalized reflectivities of four different solutions as indicated. Solid and dashed lines are the best fits calculated by Eq. (8a) and Eq. (8b), respectively. Calculations by the recursive dynamical method (exact solutions) are consistent with the DWBA. In this process, the only fitting parameter is σ or Γ which are listed in Table I. The ratios of σ and Γ shown in the

forth column of Table I are very close to the criterion ($\sigma/\Gamma = \ln 2\sqrt{\pi} \sim 1.23$ Å) for both ERF and TANH having the same exchange length, L . In other words, it means that the ED profiles from the fitting results based on ERF and TANH tend to be as close as possible, in spite of the fact that the ERF fits the data much better.

In Table I, we also note that the interfacial roughness increases with the mole-fraction of ethanol as the ST decreases, consistent with the capillary wave theory. For the interface with small roughness (i.e., pure water/air), solid (fit based on ERF) and dashed (fit based on TANH) lines start to diverge away from each other at $Q_z^2 \sim 0.2$ Å⁻² with the rest of the data (Fig. 4), which makes almost indistinguishable. However, as the roughness increases (i.e., pure ethanol), the fit to the ERF (solid lines) is much superior than that of the TANH profile (dashed line). We therefore conclude that the TANH and the EXP profiles can be clearly ruled out.

Our findings compare very well with the simulation studies that show differences between the error function and the hyperbolic tangent function [19, 20]. The error function was just marginally better than the hyperbolic tangent function[20] in fitting the interfacial density profile from molecular dynamics simulations, but yielded a sizable difference in the surface tension value such that the error function gave a more satisfactory agreement to the surface tension directly extracted from the pressure difference in the simulations. By contrast, the surface tension based on the hyperbolic tangent function always gave lower estimates. These independent studies on liquid surfaces using X-ray and MD simulations thus strongly suggest that the underlying capillary-wave dynamics dominates the profile of the liquid/vapor interface for simple liquids, and that the error-function is closest to the average effective interfacial density profile.

V. CONCLUSIONS

Using synchrotron X-ray reflectivity techniques on water/ethanol mixtures surfaces, we find that the interfacial roughness increases as surface tension decreases as expected from capillary wave theory. Modeling the experimental data to various ED profiles shows that the error-function profile is the most adequate within the experimental uncertainties for various surface tension values. Although the hyperbolic-tangent profile seems to fit the data well for small momentum transfer Q_z values, synchrotron measurements that enable large Q_z values clearly indicate the inadequacy of this profile to the bare liquid/vapor interface. We have also considered a hypothetical exponentially decaying profile that totally fails to account for X-ray reflectivity data.

Acknowledgments

The work at the Ames Laboratory was supported by the Office of Basic Energy Sciences, U.S. Department of Energy under Contract No. DE-AC02-07CH11358. Use of the Advanced Photon Source was supported by

the U. S. Department of Energy, Office of Science, Office of Basic Energy Sciences, under Contract No. DE-AC02-06CH11357. D. K was supported by the National Research Foundation (NRF) grant funded by the Korea government (MEST) No. 2011-0017435.

*email: vaknin@ameslab.gov

-
- [1] J. D. van der Waals, Z. Phys. Chem. **13**, 657 (1894).
 - [2] J. W. Cahn and J. E. Hilliard, J. Chem. Phys. **28**, 258 (1958).
 - [3] S. Fisk and B. Widom, J. Chem. Phys. **50**, 3219 (1969).
 - [4] F. P. Buff, R. A. Lovett, and F. H. Stillinger, Jr., Phys. Rev. Lett. **15**, 621 (1965).
 - [5] J. D. Weeks, J. Chem. Phys. **67**, 3106 (1977).
 - [6] M. P. Gelfand and M. E. Fisher, Physica (Amsterdam) **166A**, 1 (1990).
 - [7] F. H. Stillinger, J. Chem. Phys. **128**, 204705 (2008).
 - [8] D. Beysens and M. Robert, J. Chem. Phys. **87**, 3056 (1987).
 - [9] J. S. Huang and W. W. Webb, J. Chem. Phys. **50**, 3677 (1969).
 - [10] E. S. Wu and W. W. Webb, Phys. Rev. A **8**, 2065 (1973).
 - [11] D. G. A. L. Aarts, M. Schmidt, and H. N. W. Lekkerkerker, Science **304**, 847 (2004).
 - [12] A. Braslau, P. S. Pershan, G. Swislow, B. M. Ocko, and J. Als-Nielsen, Phys. Rev. A **38**, 2457 (1988).
 - [13] B. M. Ocko, X. Z. Wu, E. B. Sirota, S. K. Sinha, and M. Deutsch, Phys. Rev. Lett. **72**, 242 (1994).
 - [14] S. K. Sinha, E. B. Sirota, S. Garoff, and H. B. Stanely, Phys. Rev. B **38**, 2297 (1988).
 - [15] M. K. Sanyal, S. K. Sinha, K. G. Huang, and B. M. Ocko, Phys. Rev. Lett **66**, 628 (1991).
 - [16] M. Fukuto, R. K. Heilmann, P. S. Pershan, J. A. Griffiths, S. M. Yu, and D. A. Tirrell, Phys. Rev. Lett **81**, 3455 (1998).
 - [17] M. Fukuto, O. Gang, K. J. Alvine, and P. S. Pershan, Phys. Rev. E **74**, 031607 (2006).
 - [18] D. Vaknin, W. Bu, J. Sung, Y. Jeon, and D. Kim, J. Phys: Condensed Matter **21**, 115105 (2009).
 - [19] S. W. Sides, G. S. Grest, and M. D. Lacasse, Phys. Rev. E **60**, 6708 (1999).
 - [20] A. E. Ismail, G.S. Grest, and M. J. Stevens, J. Chem. Phys. **125**, 014702 (2006).
 - [21] B. A. Bauer and S. Patel, J. Chem. Phys. **131**, 084709 (2009).
 - [22] L. G. Parratt, Phys. Rev. **59**, 359 (1954).
 - [23] W. Bu, D. Vaknin, and A. Travesset, Langmuir **22**, 5673 (2006).
 - [24] Vaknin, D. In *Characterization of Materials*; Kaufmann, E. N., Ed., John Wiley & Sons: New York, 2012; Vol. 2, pp 1393-1423. (2003).